electronics

Communication

Developing PCM-Based Microwave and Millimetre-Wave Switching Networks by Optimised Building Blocks

Rodica Ramer and King Yuk Chan *

The School of Electrical Engineering and Telecommunications, The University of New South Wales, Sydney, NSW 2052, Australia
* Correspondence: kyc@unsw.edu.au

Abstract: The implementation of microwave and millimetre-wave switching networks using phase change material (PCM) is presented in this paper. We propose integrating a combination of ultra-wide bandwidth-optimised building cells into a unique semi-T type switch. The construction of arrays with different dimensions is enabled. The present paper selected GeTe for the PCM-based switches, which are 150 nm GeTe thin-film offering on- and off-state σ_{on} = 37,203,703 S/m and σ_{off} = 94.97 S/m conductivities by a customised eight-step fabrication process. The integrated semi-T switch cell with two, thru, and turn operational states allows easy expansion into the form of a staircase switch matrix. The simulated results for the semi-T type switch show excellent insertion loss of better than 0.8 dB, return loss of better than 20 dB, and isolation of 40 dB for both the thru and turn paths from DC to 120 GHz. The proposed 4 × 4 staircase switch matrix with a dimension of only 510 × 510 μm^2 is also the smallest in its class. The switch matrix exhibits better than 17 dB return loss and 40 dB isolations across all possible combinations and paths.

Keywords: phase change material (PCM); switch; switching networks; switch matrix; monolithic microwave integrated circuits

Citation: Ramer, R.; Chan, K.Y. Developing PCM-Based Microwave and Millimetre-Wave Switching Networks by Optimised Building Blocks. *Electronics* **2022**, *11*, 3683. https://doi.org/10.3390/electronics11223683

Academic Editor: Riccardo Bernardini

Received: 21 October 2022
Accepted: 9 November 2022
Published: 10 November 2022

1. Introduction

Switches represent one of the most fundamental building blocks of electronic systems. They are 'everywhere' and in 'everything'. At the same time, wireless communications systems are continually progressing and expanding to meet the demands for reliable, high-data-rate operation in multiple frequency ranges, evolving into complex hardware architectures with carrier aggregation and multiple-input multiple-output (MIMO) antennas [1]. For instance, a 4G cellular radio-frequency (RF) front end needs to support more than 16 bands, 60 RF ports, and 30 RF switches per RF port [2]. Given the rising consumer demand for wireless ubiquity and the desire for anytime, anywhere access, billions of connections are yet to be made. The 5G mobile and upcoming 6G networks expand into higher frequency ranges (from 28 GHz towards 1 THz) with massive MIMO antennas that make the RF front end much more complex and challenging. The increased complexity of RF front ends poses severe design and layout challenges where reconfigurable RF front ends and tuneable antennas are solutions to maintain the RF systems [3,4]. How these breakthrough changes to networks and telecommunications affect the switching routing and communication networks remain to be seen. An inevitable fact is that architectures of high-performance, power-aware, low-loss, linear, minimised RF switches are integral parts of these tuneable RF systems and redundancy networks.

The current state of commercial switches demonstrates that the most used mechanical and semiconductor-type switches offer numerous advantages but come with several trade-offs. Mechanical RF switches demonstrate excellent RF performance but are substantial in size and expensive. The semiconductor switches are compact but have poor linearity and signal leakage [5]. Commercial RF switches include field-effect transistors (FET), silicon on insulator (SOI), silicon on sapphire (SOS), gallium arsenide (GaAs), gallium nitride (GaN), etc., technologies and radio frequency microelectromechanical systems (RF MEMS). RF MEMS switches outperform the mechanical and semiconductor switches in terms of linearity and power handling capability and offer the best figure of merit (FOM) ($f = 1/R_{on}C_{off}$), but suffer from reliability and limited integration issues [6]. This justified the quest for reinventing the next generation of RF switch technology, where the phase change materials (PCM) are distinguished for their remarkable attributes. The latest series of PCM RF switches raises new RF switch performance standards, marking another milestone in RF devices' history [7].

Phase change materials that are currently considered for microwave applications are classified into chalcogenides alloys [8] and vanadium oxide (VO_2) [9]. Chalcogenide-based PCMs that involve one or more group VI elements, such as sulphur (S), selenium (Se), and telluride (Te), were initially known for their applications in optical storage media and non-volatile memory devices.

PCM can convert a high resistivity (in the amorphous phase) into a low resistivity state (in the crystalline phase) and vice-versa upon thermal pulse application, as illustrated in Figure 1. The thermal activation can be triggered by electrical [9] means provided by localised embedded microheaters or optical [10] by lasers. A pulse with medium amplitude (~1–2 V) and long duration (~μs) is used for crystallisation to switch the PCM to an on-state. When the PCM is in an amorphous state, the applied pulse produces sufficient heat to the PCM between its crystallisation temperature T_c and melting temperature T_m. Slowly the PCM cools down at a certain speed, and the atoms gradually rearrange in an orderly manner to finally turn into a crystalline state. Re-amorphisation requires a pulse with high amplitude (>2 V) and short duration (~ns). This pulse is applied to melt the PCM in a crystalline state above T_m, where the atoms are arranged in a disorderly manner. After rapid quenching, the atoms are frozen and remain disordered in the amorphous phase for the off-PCM switch state. Amorphisation requires a higher energy pulse to melt the material than crystallisation. A higher melting temperature than in the crystalline phase temperature is needed from the electrical pulses.

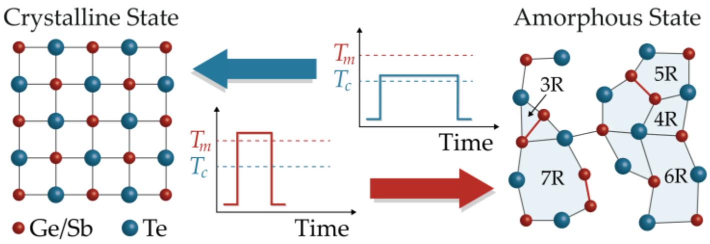

Figure 1. GeTe PCM reversible transformation using an electric pulse [8].

Critical performance parameters of RF switches include low insertion loss (IL), high isolation, excellent linearity, low power consumption, easy integration with conventional semiconductor technologies, reliability, and packaging. Large resistance contrast R_{off}/R_{on} (for an extensive dynamic range) represents an additional requirement for PCM-based switches, where R_{on} and R_{off} signify crystalline and amorphous state resistivity, respectively.

The insertion loss and isolation of up to 20 GHz of PCM switches vs MEMS, aluminium gallium arsenide (AlGaAs) diode, GaN, high-electron-mobility transistor (HEMT), complementary metal–oxide–semiconductor (CMOS), and GaAs pseudomorphic high-electron-mobility transistor (pHEMT) technologies are illustrated in Figure 2 [11]. The results show that PCM switches outperform RF MEMS and semiconductor switches with the lowest insertion loss, better than 0.23 dB. The second-best isolation (better than 35 dB) also highlights the significant potential of the RF industry for integration into complex structures. The first chalcogenide phase change material GeTe-based reconfigurable switch was presented in [12].

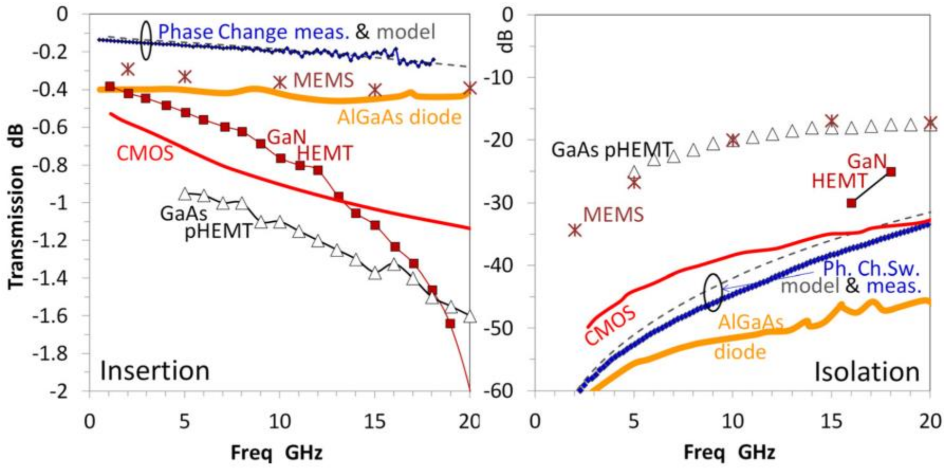

Figure 2. RF performance comparison between various RF switch technologies [11].

Recently, GeTe-based switches were reported by Wang, M. from the University of Michigan [13], El-Hinnawy, N. from Northrop Grumman Corp. [11,14] (Figure 3a), and Moon, J. from HRL Laboratories [15] (Figure 3b). Most of these switches have a 10–12 THz FOM with good RF performance [16]. Apart from single-pole single-throw (SPST) RF PCM switches, Northrop Grumman Corp. also reported a PCM GeTe-based single-pole double-throw (SPDT) switch for millimetre-wave applications [11], shown in Figure 3c. An ongoing body of work targeting better than the currently available RF performance of the RF switches (including the semiconductor) followed. Improvements in many different parameters, such as power handling capability [17], linearity and extended operating frequency range to millimetre-waves [18], and advancements of four-port switches [19–23], etc., were further examined recently.

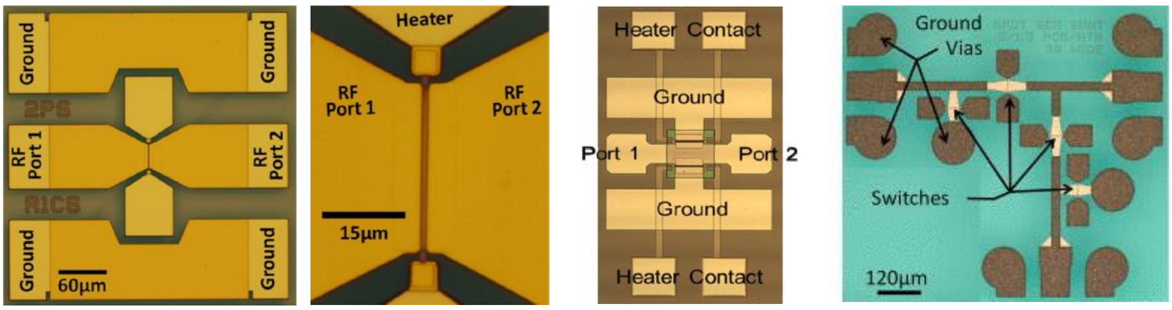

(**a**) (**b**) (**c**)

Figure 3. Optical micrographs. (**a**) PCM RF series switch [11]; (**b**) GeTe RF shunt switch [15]; (**c**) GeTe RF SPDT switch [11].

PCM offers more than five orders of resistance change with nanosecond voltage pulses, establishing this technology as ideal for low loss at microwave and mm-wave frequencies. The already developed devices provide the versatility of reduced device area by dense integration of switching unit cells [23–25], increased reliability due to the lack of moving parts, and good performance up to 67 GHz [18–25]. PCM also demonstrated its versatility with applications in many other areas, such as in solar energy [26].

This paper presents state-of-the-art, highly miniaturised, easily integrated with other RF circuits latching switches with negligible direct current (DC) power consumption. We demonstrate the details of the excellent S-parameters of the innovative built models of (a) an RF single-pole single-throw (SPST) switch in a series configuration, (b) a semi-T switch, and (c) a 4 $\times$ 4 staircase switch matrix.

2. Fabrication Process

The first step is to identify the best available PCM material for microwave applications, particularly for microwave switches, as trial devices and fundamental enabling circuit elements. Germanium–telluride (GeTe) is the most significant contender for low-cost and low-loss broadband mm-wave components. Newly developed PCM GeTe-based RF switches have outperformed currently available state-of-the-art semiconductor devices [7]. Antimony–telluride (SbTe) has also been successfully implemented in RF applications, while promising indium–antimony–telluride (InSbTe) and silicon–antimony–telluride (SiSbTe)-based alloys require further RF performance investigation and possible implementation [27,28]. A comparison among GeTe [7,29], Sb(Te) [3], and VO_2 [30]-based SPST switches reveal that GeTe currently outperforms all. We also identified a wide range of other PCM materials providing superior properties and their potential for high-frequency applications, as shown in Table 1. GeTe and $Ge_2Sb_2Te_5$ (GST) are also included in the table for a quick comparison. One may notice many vacant entries in the table, mainly due to the currently [31–37] unexplored and, thus, unavailable data in the literature . We expect this table to expand in the next couple of years with missing and extra content. Currently, the compound $Si_{10.7}Sb_{39.5}Te_{49.8}$ has desirable properties of an RF switch, including a high OFF to ON resistivity ratio of 7th order and an additional property of minimal thickness reduction of 1.7% when crystallised cf. 6.8% of GST. This may benefit larger operating lifetimes, improving its reliability as the cyclic expansion and contraction are smaller. GeSeTl also has the same desirable property with an 8th order resistivity ratio. However, due to the ease of access to materials and their microwave parameters, all our designs are GeTe-based.

Table 1. List of PCM materials for comparison.

Material	On (Ωcm)	Off (Ωcm)	Off/On	T_{cryst} (°C)	T_{melt} (°C)	Mechanism
GeTe	2×10^{-4}	10^3	5×10^6	>170	735	Heat
$Ge_2Sb_2Te_5$ (GST)	1×10^{-2}	1×10^2	1×10^4	162–616	641	Heat
$Si_{10.7}Sb_{39.5}Te_{49.8}$ [31]	2.5	2.5×10^7	1×10^7	>200	<600	Heat
$Si_{15}Te_{85\text{-}x}Bi_x$ [32]		$1.5 - 3 \times 10^6$				Heat
$Si_{20}Te_{80\text{-}x}Bi_x$ [33]		$1.5 - 3 \times 10^6$				Heat
$Si_{20}Te_{80}Sn_x$ [34]		$0.6 - 1.6 \times 10^6$		250		Heat
SeTe [35]		2×10^6		~400		Heat
Se_3Te [35]		5×10^8		~400		Heat
As_2Se_3 [36]		3.3×10^{10}				Heat
GeSeTl [37]			4×10^8			Heat

The tailored PCM microfabrication process based on our well-developed RF MEMS fabrication at the UNSW is illustrated in Figure 4 [38]. High-performance microwave, mm-wave substrates, alumina with ε_r = 9.8, 635 µm thick, are used as the carrying substrate.

1. A resistive layer used for PCM's microwave resistors or heaters is deposited and patterned. A 70 nm layer of tungsten (W) is sputtered at 850 °C and patterned using reactive ion etching (RIE);
2. A thin isolation/barrier layer of 50 nm silicon nitride (SiN_x) is deposited by plasma-enhanced chemical vapour deposition (PECVD);
3. A thin PCM layer is deposited. A 150 nm thick PCM is DC sputtered and patterned using the lift-off technique, followed by an annealing process;
4. The first RF metal layer, 1 µm of gold (Au) layer, is DC sputtered together will 50 nm of titanium (Ti) for better adhesion. A lift-off process is used to pattern these;
5. A second isolation layer, silicon dioxide (SiO_2), primarily for MIM capacitors, is PECVD deposited, followed by patterning with diluted hydrofluoric acid (HF). HF is

selected to remove the SiO_2 as it etches SiO_2 at a much higher rate than the previously deposited SiN_x and all other materials exposed at the surface;
6. A sacrificial layer, polyimide, of 2.5 µm is spun on, patterned, and baked;
7. A second RF metal layer (Au/Ti) is DC sputtered and patterned by the lift-off technique. This RF signal layer is primarily for airbridges and MIM capacitors.

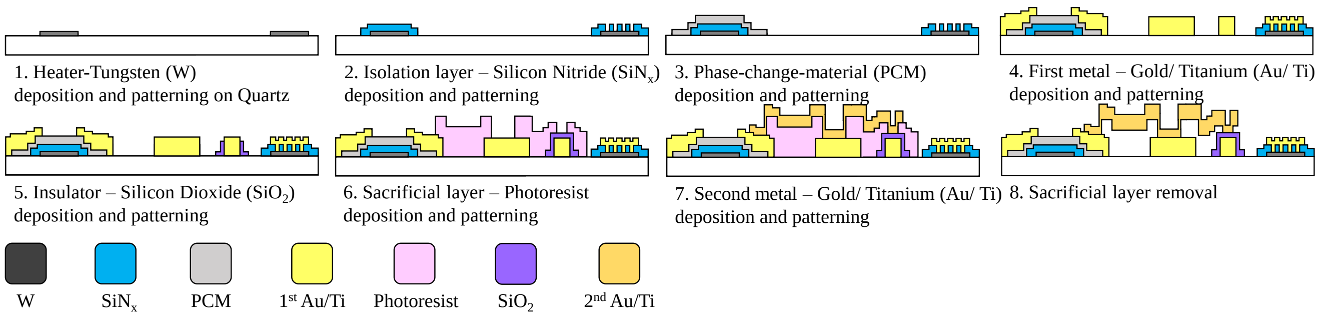

Figure 4. Our proposed standard PCM-based fabrication process.

3. Design and Methodology

An HFSS 3D view of a PCM SPST series-type switch is illustrated in Figure 5. The designs are based on the proposed fabrication process, with the materials' properties and thickness details as follows. In all cases, alumina (Al2O3) substrate ε_r = 9.8, 635 µm thick, and coplanar waveguide (CPW) 1 µm thick gold transmission lines were used. Tungsten (W) 70 nm and silicon nitride (SiN_x) 50 nm layers were used for the microheater and barrier. The chosen 150 nm GeTe thin-film conductivities were measured by a four-point probe, with on- and off-state σ_{on} = 37,203,703 S/m and σ_{off} = 94.97 S/m. The PCM-based SPST series switch is a four-terminal device with two terminals for RF signal flow and two terminals (bias) for providing electrical pulses connected to the embedded microheater. The microheater's width (w_h) is a crucial design parameter, as it must have a minimum feature in the design. It also determines the signal line separation that governs the on-state insertion loss (IL) and off-state isolation (Iso). Figure 6 shows the simulated PCM-based SPST RF performance. As shown in Figure 6a, as w_h increases, IL and return loss (RL) worsen. The inverse happens with the isolation when w_h varies between 0.5 µm to 2 µm, as seen in Figure 6b. It should be noted that these SPST simulation results demonstrate excellent RF behaviour up to 120 GHz, outperforming any existing technology. We further examine the simulation results and extract the actual loss after removing the mismatch loss from Figure 6a. It is worth mentioning in Figure 6c that the IL are represented by the dashed lines, showing only the contribution of the PCM and metal losses. The figure suggests a possible operation with IL as little as <0.4 dB and Iso at least >30 dB from DC to 120 GHz, even when a wider w_h must be selected. IL and Iso could further enhance operation at even higher frequencies with improved PCM materials under investigation.

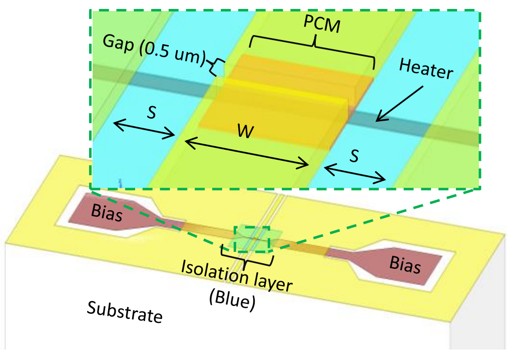

Figure 5. PCM SPST-simulated HFSS 3D model with features.

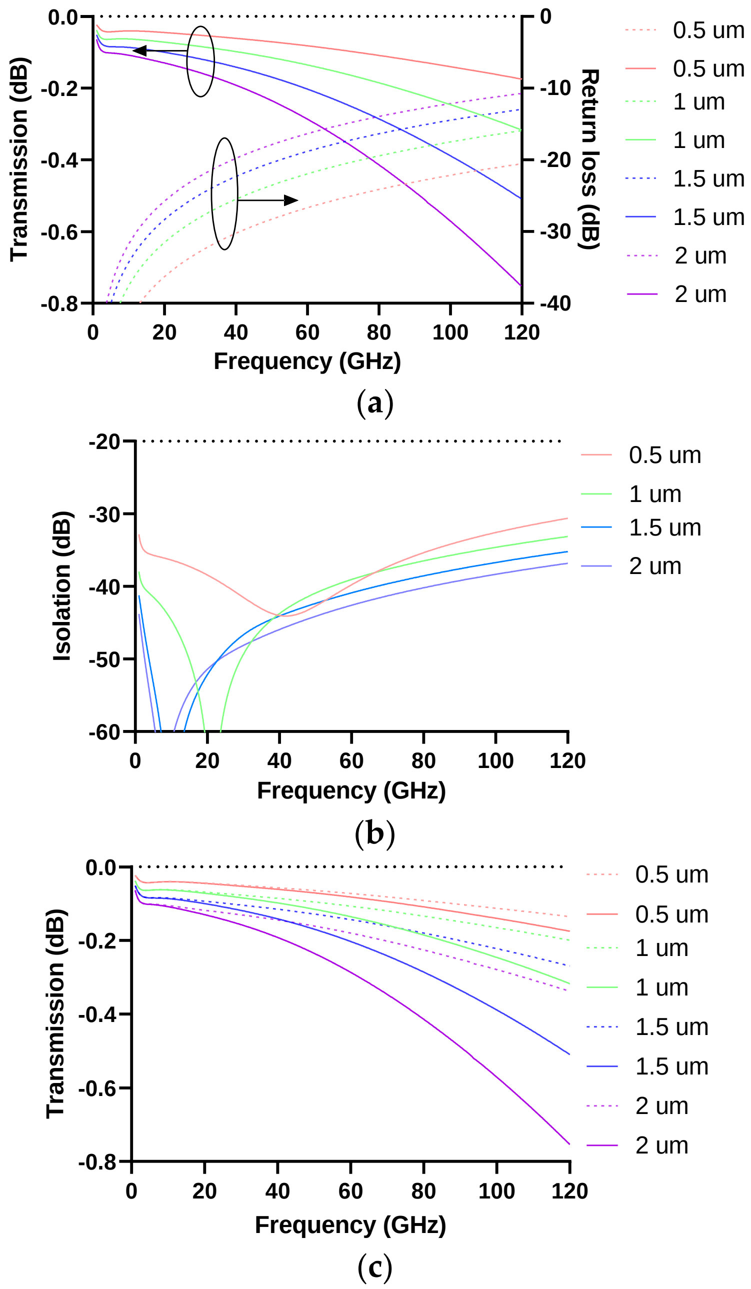

Figure 6. PCM switch simulation results vs. microheater width w_h (**a**) on-state, (**b**) off-state, and (**c**) on-state with dashed lines showing the insertion loss after removing the mismatch loss.

The PCM semi-T switch, a four-port device with two operational states, 'thru' and 'turn', is achieved by combining several infrastructure elements, 8 × SPST, a crossover (Figure 7a), 4 × T-junction (Figure 7b), and 2 × 90° turn (Figure 7c). Each infrastructure element must be designed and optimised with the best performance for wideband operation, as per our RF MEMS article [39–41]. Figure 7d shows the simulated model with the PCM switches grouped according to their operational state, thru and turn, with the full semi-T switch size of only 170 µm × 170 µm. Figure 7c,d shows the simulation results of the thru-state and turn-state. From the simulation RF performance, it can be concluded that the semi-T switch achieves the best wideband performance, unmatched by other technologies. Both states have better than 1 dB insertion loss, and better than 20 dB return loss, and the disconnected ports have better than 44 dB isolation from DC to 120 GHz.

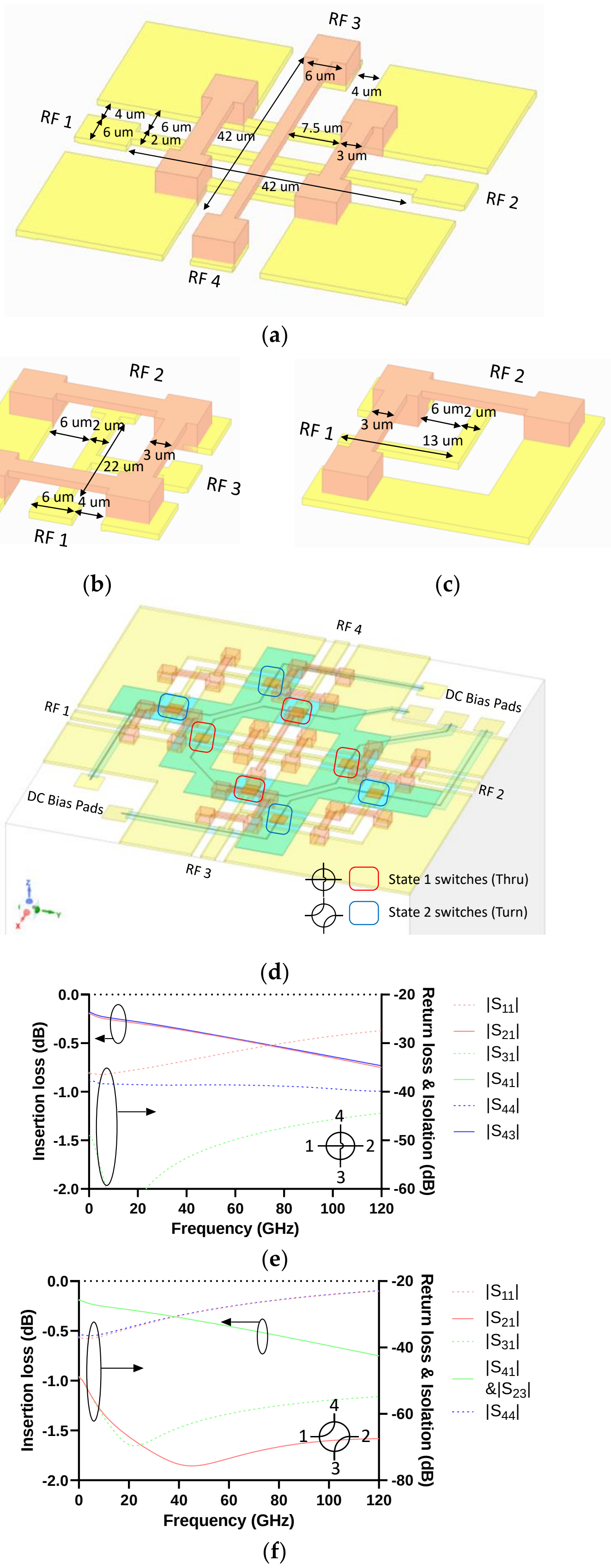

Figure 7. HFSS models of (**a**) a crossover, (**b**) a T-junction, (**c**) 90° turn, (**d**) a full model of the PCM semi-T switch based on SPST switches grouped by thru and turn operational states, (**e**) thru-state, and (**f**) turn-state simulations S-parameters.

The staircase switch matrix topology is chosen to demonstrate its smallest physical size with minimal numbers of building blocks and scalability. The staircase switch matrix is designed and assembled using the semi-T switch building block and the 90° turn with an overall dimension of 510 μm × 510 μm. Compared to a crossbar topology, for example, the staircase only requires $N(N-1)/2$ building blocks instead of $N^2 - 1$, where N is the matrix dimension, resulting in almost $\frac{1}{2}$ of the physical size. For demonstration, a 4 × 4 PCM-based staircase switch is designed and simulated. Figure 8a shows its physical layout and Figure 8b demonstrates four configurations covering all the possible paths. All four sets of connections, set 1 (IN 1 → OUT 1 (I1/O1), IN 1 → OUT 2 (I1/O2), IN 3 → OUT 3 (I3/O3), IN 4 → OUT 4 (I4/O4)), set 2 (I1/O2, I2/O1, I3/O4, I4/O3), set 3 (I1/O3, I2/O4, I3/O2, I4/O1), and set 4 (I1/O4, I2/O3, I3/O1, I4/O2) are simulated as shown in Figure 8c,d, Figures 9 and 10, respectively. Figure 8c,d, Figures 9 and 10 (i) illustrate the connected ports' insertion losses and disconnected ports' isolations, (ii) display all ports' return losses, and (iii) show the connected paths' phases vs. frequencies. In set 1, the maximum insertion losses vary from 0.9 dB to 3.98 dB, while the isolations and return losses are better than 40 dB and 20 dB, respectively, with the maximum phase difference of 294 degrees between all paths across the frequencies of interest. In set 2, a similar trend is observed, with the maximum insertion losses differing from 1.6 dB to 4 dB, and a most significant phase difference of 221 degrees. Between all ports, the isolations are still 40 dB, while the return losses at I1 and O2 ports degrade to 16 dB instead of 20 dB at other ports at 120 GHz. For sets 3 and 4, one can notice that the insertion losses variation reduces to less than 0.2 dB, with the maximum insertion losses ranging from 2.3 dB to 2.5 dB. This is due to the similar path lengths across all the connected ports. The reduced path length difference is verified by the maximum phase variation between the connected paths in these sets, which is only 63 degrees at 120 GHz. It should be noted that the isolations between all ports in sets 3 and 4 are better than 40 dB, while only ports I1, O2, and O3 in set 3 and port O1 have degraded return loss to 16 dB, while all other ports are better than 20 dB from DC to 120 GHz. It can be concluded that the 4 × 4 staircase switch matrix exhibits outstanding RF performance with return losses better than 17 dB in all sets across all ports from DC to 120 GHz. In all cases, the port-to-port isolations are better than 40 dB between all the disconnected ports across the frequency band of interest. Figure 11 shows the insertion losses and phase lengths of all possible paths of the 4 × 4 staircase switch matrix. These simulations demonstrate, for the first time, a microwave switch matrix capable of operating up to 120 GHz with the worst-case insertion loss of better than 4 dB.

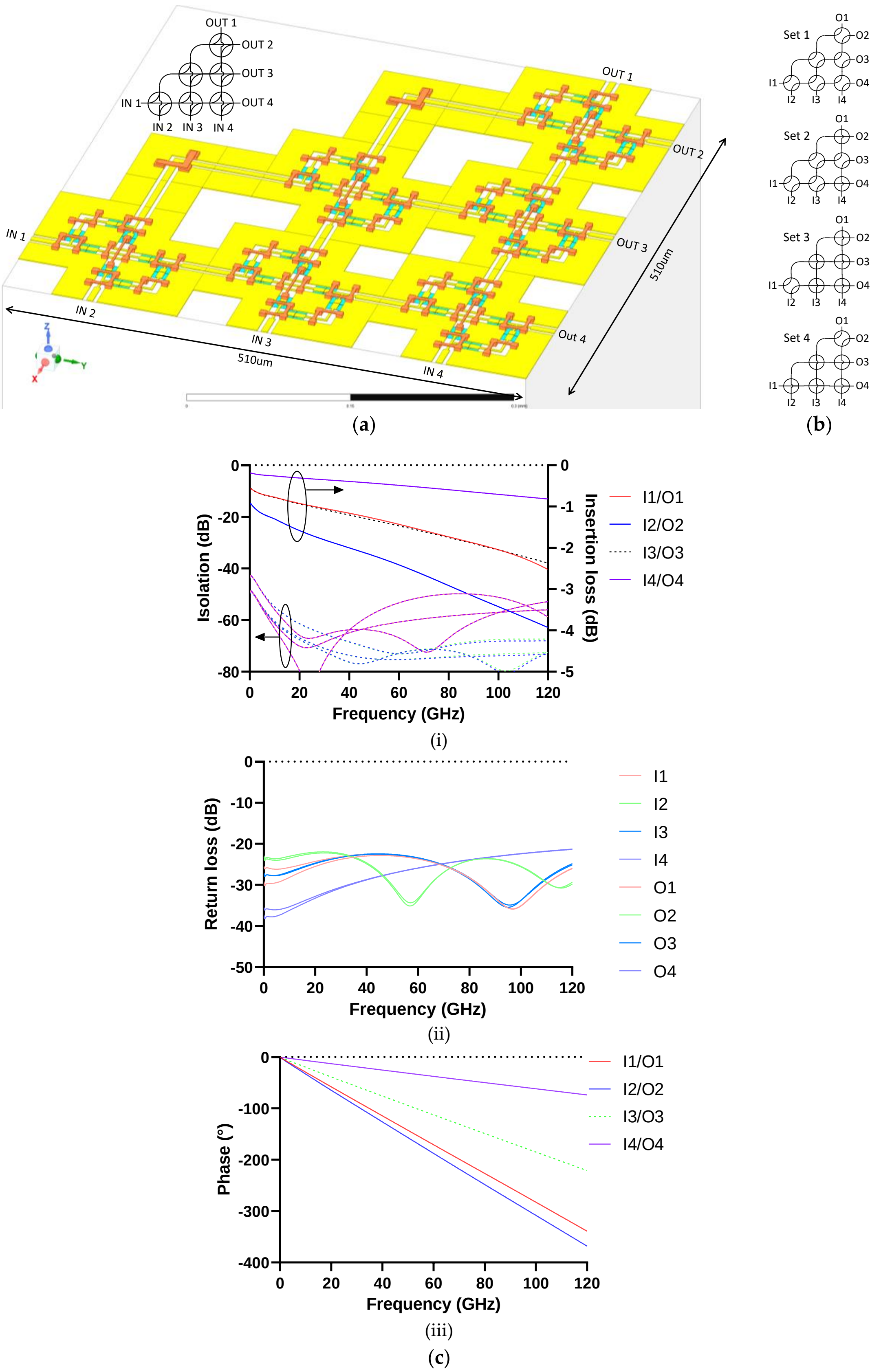

Figure 8. *Cont.*

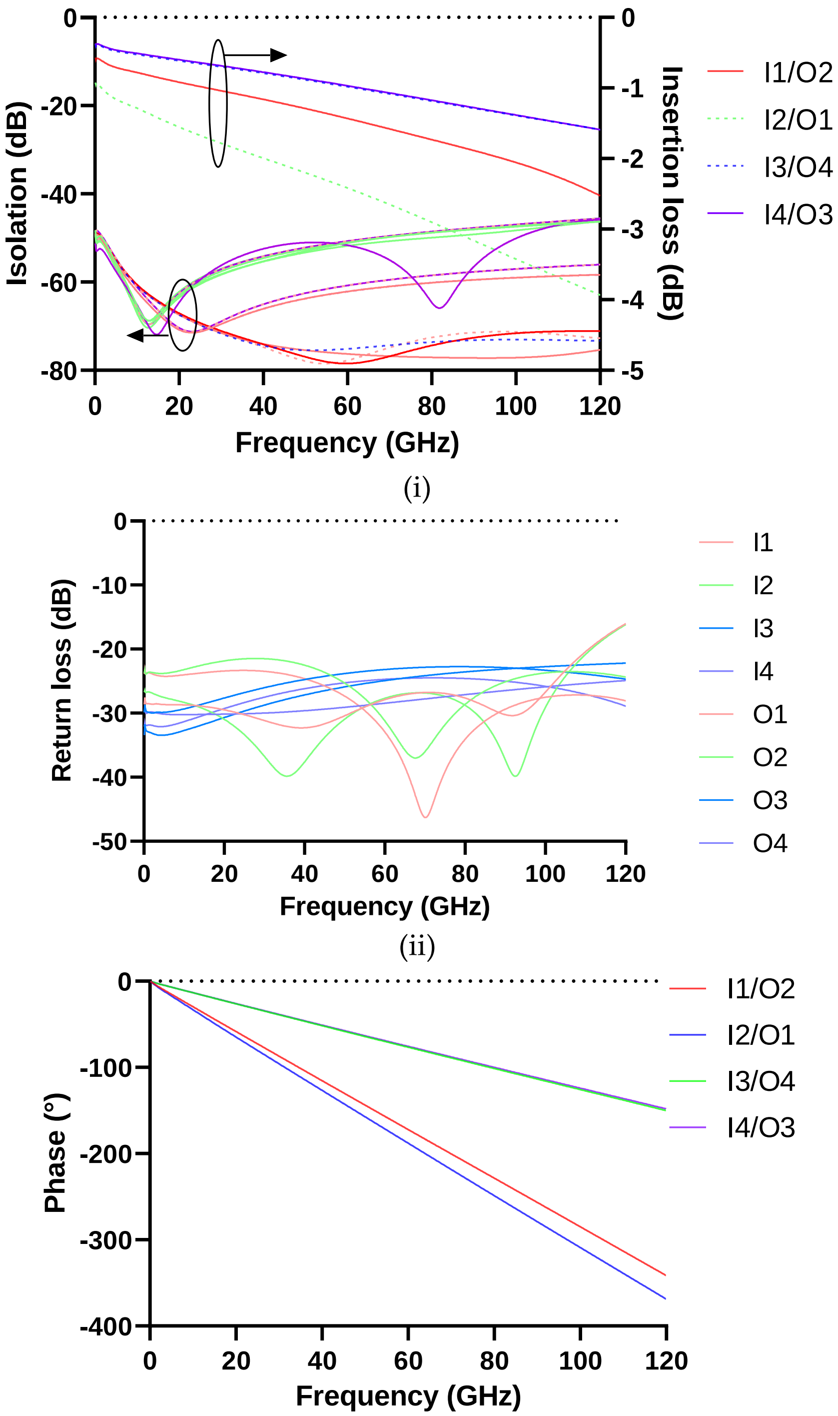

(i)

(ii)

(iii)

(**d**)

Figure 8. (**a**) Simulated HFSS model of the 4 × 4 staircase PCM-based switch matrix, (**b**) the 4 sets of configurations covering all the possible connections of, (**c**) set 1 with (i) showing the insertion losses of the connected paths and isolations between the disconnected ports, (ii) the return losses at all ports and (iii) the connected paths' phases and (**d**) set 2 RF performances with (i) showing the insertion losses of the connected paths and isolations between the disconnected ports, (ii) the return losses at all ports and (iii) the connected paths' phases. It should be noted that no legends are included for the port-to-port isolations due to the large number of disconnected ports.

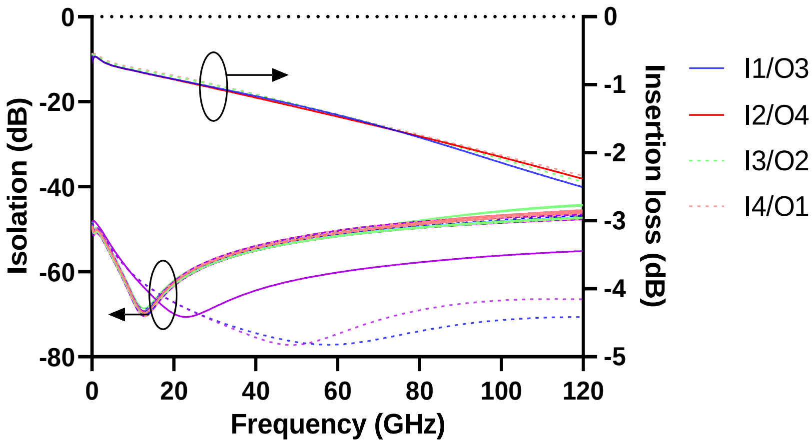

(i)

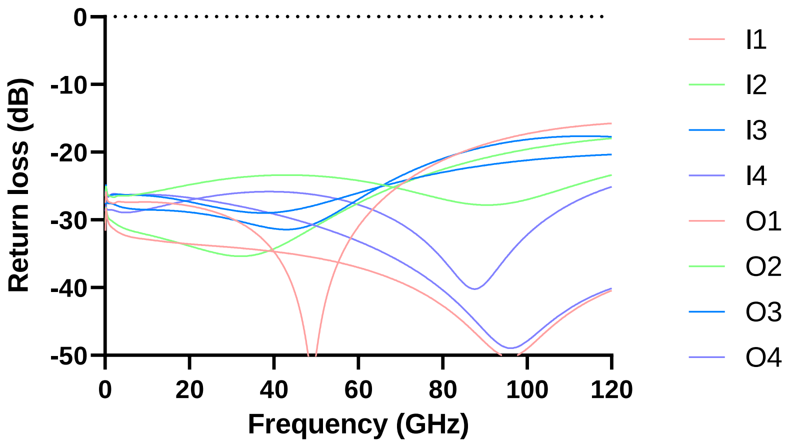

(ii)

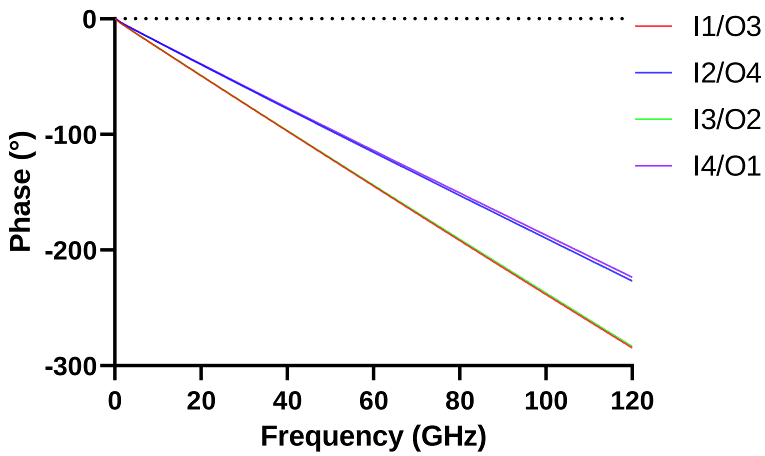

(iii)

Figure 9. RF performance of set 3 with (i) showing the insertion losses of the connected paths and isolations between the disconnected ports, (ii) the return losses at all ports and (iii) the connected paths' phases. It should be noted that no legends are included for the port-to-port isolations due to a large number of disconnected ports.

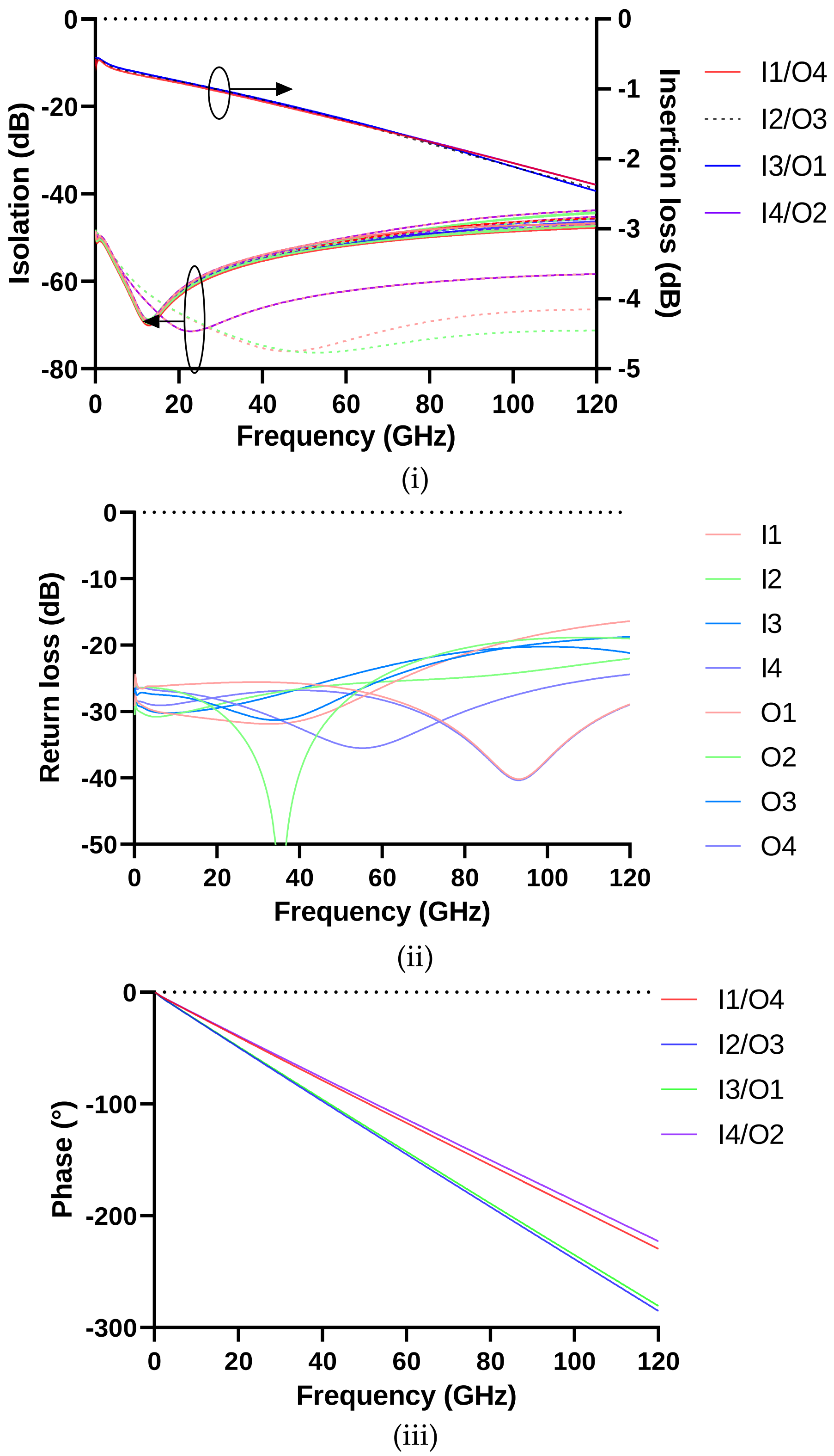

Figure 10. RF performance of set 4 with (i) showing the insertion losses of the connected paths and isolations between the disconnected ports, (ii) the return losses at all ports and (iii) the connected paths' phases. It should be noted that no legends are included for the port-to-port isolations due to a large number of disconnected ports.

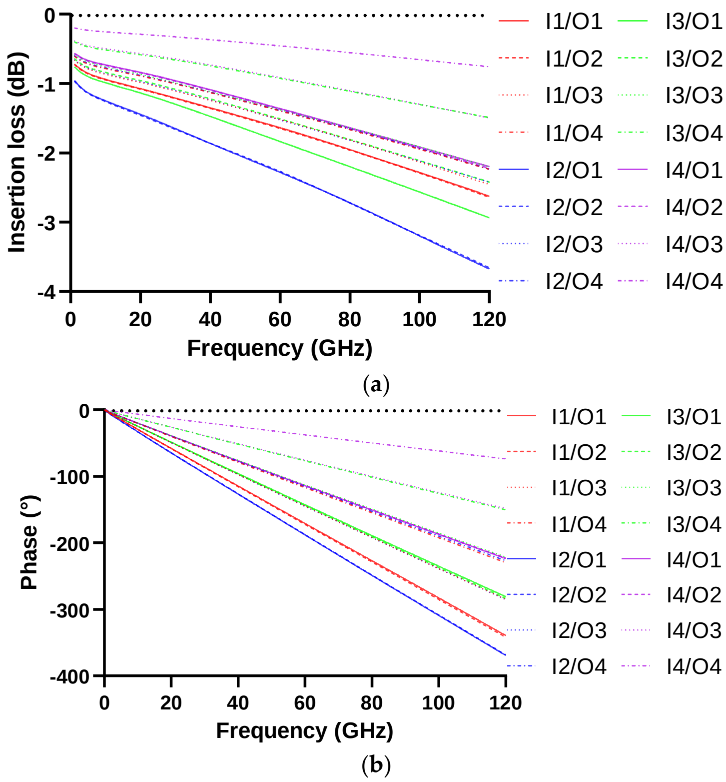

Figure 11. Simulated (**a**) insertion losses and (**b**) phase lengths (in degree) of all the connections of the 4 × 4 staircase switch matrix.

4. Conclusions

A PCM-based switching network implementation method based on optimising individual building blocks is proposed, together with its fabrication method. These building blocks are used to construct an ultra-wideband semi-T switch for a large switch matrix that can operate up to 120 GHz for the first time. The semi-T switch offers better than 0.7 dB insertion loss, 20 dB return loss, and 40 dB isolations in both the thru and turn states. As a demonstration, a 4 × 4 staircase switch matrix is shown with all its possible connection paths simulated. A 4 × 4 switching network that can operate from DC to 120 GHz with excellent RF performance is demonstrated for the first time. Better than 17 dB return loss and better than 40 dB isolations are achieved for all ports. To the best of the authors' knowledge, this is the first PCM-based staircase switch matrix ever reported, and it outclasses all existing technologies.

Author Contributions: Conceptualization, R.R. and K.Y.C.; methodology, R.R. and K.Y.C.; software, K.Y.C.; validation, R.R. and K.Y.C.; formal analysis, R.R. and K.Y.C.; investigation, R.R. and K.Y.C.; resources, R.R. and K.Y.C.; data curation, K.Y.C.; writing—original draft preparation, R.R. and K.Y.C.; writing—review and editing, R.R. and K.Y.C.; visualization, K.Y.C.; supervision, R.R.; project administration, R.R.; funding acquisition, R.R. All authors have read and agreed to the published version of the manuscript.

Funding: This research received no external funding.

Conflicts of Interest: The authors declare no conflict of interest.

References

1. You, X.; Wang, C.-X.; Huang, J.; Gao, X.; Zhang, Z.; Wang, M.; Huang, Y.; Zhang, C.; Jiang, Y.; Wang, J.; et al. Towards 6G wireless communication networks: Vision, enabling technologies, and new paradigm shifts. *Sci. China Inf. Sci.* **2020**, *64*, 110301. [CrossRef]
2. Campbell, C.F.; Dumka, D.C. Wideband High Power GaN on SiC SPDT Switch MMICs. In Proceedings of the 2010 IEEE/MTT-S International Microwave Symposium—IMS, Anaheim, CA, USA, 23–28 May 2010; pp. 145–148.

3. Moon, J.S.; Seo, H.C.; Son, K.A.; Lee, K.; Zehnder, D.; Tai, H. 5 THz Figure-of- Merit Reliable Phase-change RF Switches for Millimeter-wave Applications. In Proceedings of the 2018 IEEE/MTT-S International Microwave Symposium—IMS, Philadelphia, PA, USA, 10–15 June 2018; pp. 836–838.
4. Seki, T.; Yamamoto, J.; Murakami, A.; Yoshitake, N.; Hinuma, K.-I.; Fujiwara, T.; Sano, K.; Matsushita; Sato, F.; Oba, M. An RF MEMS switch for 4G Front-Ends. In Proceedings of the 2013 IEEE MTT-S International Microwave Symposium Digest (MTT), Seattle, WA, USA, 2–7 June 2013; pp. 1–3.
5. Grant, P.D.; Denhoff, M.W.; Mansour, R.R. A Comparison between RF MEMS Switches and Semiconductor Switches. In Proceedings of the 2004 International Conference on MEMS, NANO and Smart Systems (ICMENS'04), Banff, AB, Canada, 25–27 August 2004; pp. 515–521.
6. Rebeiz, G.M.; Patel, C.D.; Han, S.K.; Ko, C.H.; Ho, K.M.J. The Search for a Reliable MEMS Switch. *IEEE Microw. Mag.* **2013**, *14*, 57–67. [CrossRef]
7. Wainstein, N.; Adam, G.; Yalon, E.; Kvatinsky, S. Radiofrequency Switches Based on Emerging Resistive Memory Technologies—A Survey. *Proc. IEEE* **2021**, *109*, 77–95. [CrossRef]
8. Singh, T.; Mansour, R.R. Characterisation, Optimisation, and Fabrication of Phase Change Material Germanium Telluride Based Miniaturized DC–67 GHz RF Switches. *IEEE Trans. Microw. Theory Tech.* **2019**, *67*, 3237–3250. [CrossRef]
9. Crunteanu, A.; Orlianges, J.C.; Bessaudou, A. Fast optical activation of insulator-to-metal transition in vanadium dioxide phase changed materials. *Oxide-Based Mater. Devices* **2020**, *11281*, 95–101.
10. Leon-Valdes, J.; Huitema, L.; Arnaud, E.; Passerieux, D.; Crunteanu, A. Polarization Reconfiguration of a Millimeter-Waves Antenna using the Optical Control of Phase Change Materials. In Proceedings of the 2020 14th European Conference on Antennas and Propagation (EuCAP), Copenhagen, Denmark, 15–20 March 2020; pp. 1–4.
11. El-Hinnawy, N.; Borodulin, P.; Wagner, B.P.; King, M.R.; Jones, E.B.; Howell, R.S.; Lee, M.J.; Young, R.M. Low-loss latching microwave switch using thermally pulsed non-volatile chalcogenide phase change materials. *Appl. Phys. Lett.* **2014**, *105*, 13501. [CrossRef]
12. Chua, E.K.; Shi, L.P.; Zhao, R.; Lim, K.G.; Chong, T.C.; Schlesinger, T.E.; Bain, J.A. Low resistance, high dynamic range reconfigurable phase change switch for radio frequency applications. *Appl. Phys. Lett.* **2010**, *97*, 183506. [CrossRef]
13. Wang, M.; Lin, F.; Rais-Zadeh, M. Need a Change? Try GeTe: A Reconfigurable Filter Using Germanium Telluride Phase Change RF Switches. *IEEE Microw. Mag.* **2016**, *17*, 70–79. [CrossRef]
14. El-Hinnawy, N.; Borodulin, P.; Jones, E.B.; Wagner, B.P.; King, M.R.; Mason, J.S.; Bain, J.; Paramesh, J.; Schlesinger, T.E.; Howell, R.S.; et al. 12.5 THz Fco GeTe Inline Phase-Change Switch Technology for Reconfigurable RF and Switching Applications. In Proceedings of the 2014 IEEE Compound Semiconductor Integrated Circuit Symposium (CSICS), La Jolla, CA, USA, 19–22 October 2014; pp. 1–3.
15. Moon, J.S.; Seo, H.C.; Le, D.; Fung, H.; Schmitz, A.; Oh, T.; Kim, S.; Son, K.A.; Yang, B. 10.6 THz figure-of-merit phase-change RF switches with embedded micro-heater. In Proceedings of the 2015 IEEE 15th Topical Meeting on Silicon Monolithic Integrated Circuits in RF Systems, San Diego, CA, USA, 26–28 January 2015; pp. 73–75.
16. Slovin, G.; Xu, M.; Singh, R.; Schlesinger, T.E.; Paramesh, J.; Bain, J.A. Design Criteria in Sizing Phase-Change RF Switches. *IEEE Trans. Microw. Theory Tech.* **2017**, *65*, 4531–4540. [CrossRef]
17. Singh, T.; Mansour, R.R. Investigation into Self Actuation Limitation and Current Carrying Capacity of Chalcogenide Phase Change GeTe-Based RF Switches. *IEEE Trans. Electron Devices* **2020**, *67*, 5717–5722. [CrossRef]
18. Singh, T.; Mansour, R.R. Experimental Investigation of Performance, Reliability, and Cycle Endurance of Nonvolatile DC–67 GHz Phase-Change RF Switches. *IEEE Trans. Microw. Theory Tech.* **2021**, *69*, 4697–4710. [CrossRef]
19. Singh, T.; Mansour, R.R. Ultra-Compact Phase-Change GeTe-Based Scalable mmWave Latching Crossbar Switch Matrices. *IEEE Trans. Microw. Theory Tech.* **2022**, *70*, 938–949. [CrossRef]
20. Singh, T.; Mansour, R.R. Miniaturized DC–60 GHz RF PCM GeTe-Based Monolithically Integrated Redundancy Switch Matrix Using T-Type Switching Unit Cells. *IEEE Trans. Microw. Theory Tech.* **2019**, *67*, 5181–5190. [CrossRef]
21. Singh, T.; Mansour, R.R. Scalable Non-Volatile Chalcogenide Phase Change GeTe-Based Monolithically Integrated mmWave Crossbar Switch Matrix. In Proceedings of the 2021 IEEE MTT-S International Microwave Symposium (IMS), Los Angeles, CA, USA, 7–25 June 2021; pp. 420–423.
22. Singh, T.; Mansour, R.R. Monolithic PCM Based Miniaturized T-type RF Switch for Millimeter Wave Redundancy Switch Matrix Applications. In Proceedings of the 2019 IEEE MTT-S International Microwave Symposium (IMS), Boston, MA, USA, 2–7 June 2019; pp. 658–660.
23. Singh, T.; Mansour, R.R. A Miniaturized Monolithic PCM Based Scalable Four-Port RF Switch Unit-Cell. In Proceedings of the 2019 49th European Microwave Conference (EuMC), Paris, France, 1–3 October 2019; pp. 180–183.
24. Singh, T.; Mansour, R.R. Chalcogenide Phase Change Material GeTe Based Inline RF SPST Series and Shunt Switches. In Proceedings of the 2018 IEEE MTT-S International Microwave Workshop Series on Advanced Materials and Processes for RF and THz Applications (IMWS-AMP), Ann Arbor, MI, USA, 16–18 July 2018; pp. 1–3.
25. Singh, T.; Mansour, R.R. Characterization of Phase Change Material Germanium Telluride for RF Switches. In Proceedings of the 2018 48th European Microwave Conference (EuMC), Madrid, Spain, 23–27 September 2018; pp. 475–478.
26. Selimefendigil, F.; Öztop, H.F. Mixed convection in a PCM filled cavity under the influence of a rotating cylinder. *Solar Energy* **2020**, *200*, 61–75. [CrossRef]

27. Hawasli, S.H.; Cruz, L.D.L.; El-Hinnawy, N.; Borodulin, P.; King, M.; Young, R.M.; Zaghloul, M.; Ivanov, T.G. Investigation of on-state power handling dependence on number of cycles for germanium telluride RF switches. In Proceedings of the 2017 IEEE MTT-S International Microwave Symposium (IMS), Honolulu, HI, USA, 4–9 June 2017; pp. 292–295.
28. Cruz, L.D.L.; Birdwell, A.G.; Zaghloul, M.; Ivanov, T.G. GeTe Phase Change Research at the US Army Research Laboratory. In Proceedings of the 2018 IEEE/MTT-S International Microwave Symposium—IMS, Philadelphia, PA, USA, 10–15 June 2018; pp. 843–845.
29. Moon, J.-s.; Seo, H.-c.; Son, K.-a.; Lee, K.; Zehnder, D.; Tai, H.; Le, D. Phase-change RF switches with robust switching cycle endurance. In Proceedings of the 2018 IEEE Radio and Wireless Symposium (RWS), Anaheim, CA, USA, 15–18 January 2018; pp. 231–233.
30. Mennai, A.; Bessaudou, A.; Cosset, F.; Guines, C.; Passerieux, D.; Blondy, P.; Crunteanu, A. High Cut-off Frequency RF Switches integrating a Metal-Insulator Transition Material. In Proceedings of the IEEE MTT-S International Microwave Symposium, Phoenix, AZ, USA, 17 May 2015.
31. Qiao, B.; Feng, J.; Lai, Y.; Cai, Y.; Lin, Y.; Tang, T.-a.; Cai, B.; Chen, B. Si–Sb–Te films for phase-change random access memory. *Semicond. Sci. Technol.* **2006**, *21*, 1073–1076. [CrossRef]
32. Jeevan Fernandes, B.; Munga, P.; Ramesh, K.; Udayashankar, N.K. Electrical switching and thermal behavior of ternary $Si_{15}Te_{85}$-xBix ($0 \leq x \leq 2$) chalcogenide glasses. *Mater. Today Proc.* **2018**, *5*, 21292–21298. [CrossRef]
33. Fernandes, B.J.; Ramesh, K.; Udayashankar, N.K. Electrical switching in $Si_{20}Te_{80}-xBix$ ($0 \leq x \leq 3$) chalcogenide glassy alloys. *J. Non-Cryst. Solids* **2018**, *483*, 86–93. [CrossRef]
34. Jagannatha, K.B.; Roy, D.; Das, C. Electrical switching and crystalline peak studies on Si20Te80−xSnx ($1 \leq x \leq 7$) chalcogenide bulk glasses. *J. Non-Cryst. Solids* **2020**, *544*, 120196. [CrossRef]
35. Sharma, V.; Sharda, S.; Sharma, N.; Katyal, S.C.; Sharma, P. Chemical ordering and electronic properties of lone pair chalcogenide semiconductors. *Prog. Solid State Chem.* **2019**, *54*, 31–44. [CrossRef]
36. Shaw, R.F.; Liang, W.Y.; Yoffe, A.D. Optical properties, photoconductivity, and energy levels in crystalline and amorphous arsenic triselenide. *J. Non-Cryst. Solids* **1970**, *4*, 29–42. [CrossRef]
37. Kotkata, M.F.; Afifi, M.A.; Labib, H.H.; Hegab, N.A.; Abdel-Aziz, M.M. Memory switching in amorphous Ge·Se·Tl chalcogenide semiconductor films. *Thin Solid Film* **1994**, *240*, 143–146. [CrossRef]
38. Li, X.; Chan, K.Y.; Ramer, R. E-Band RF MEMS Differential Reflection-Type Phase Shifter. *IEEE Trans. Microw. Theory Tech.* **2019**, *67*, 4700–4713. [CrossRef]
39. Chan, K.Y.; Ramer, R.; Mansour, R.R. Novel Miniaturized RF MEMS Staircase Switch Matrix. *IEEE Microw. Wirel. Compon. Lett.* **2012**, *22*, 117–119. [CrossRef]
40. Chan, K.Y.; Mansour, R.R.; Ramer, R. Miniaturized RF MEMS switch cells for crossbar switch matrices. In Proceedings of the 2010 Asia-Pacific Microwave Conference, Yokohama, Japan, 7–10 December 2010; pp. 1829–1832.
41. Chan, K.Y.; Daneshmand, M.; Mansour, R.R.; Ramer, R. Scalable RF MEMS Switch Matrices: Methodology and Design. *IEEE Trans. Microw. Theory Tech.* **2009**, *57*, 1612–1621. [CrossRef]